Supplement of Clim. Past, 22, 585–604, 2026
https://doi.org/10.5194/cp-22-585-2026-supplement

Climate of the Past
Open Access
EGU

Supplement of

New isoprenoid GDGT index as a water mass and temperature proxy in the Southern Ocean

Hana Ishii et al.

Correspondence to: Hana Ishii (hana.ishii@vuw.ac.nz) and Osamu Seki (seki@lowtem.hokudai.ac.jp)

Supplement figures

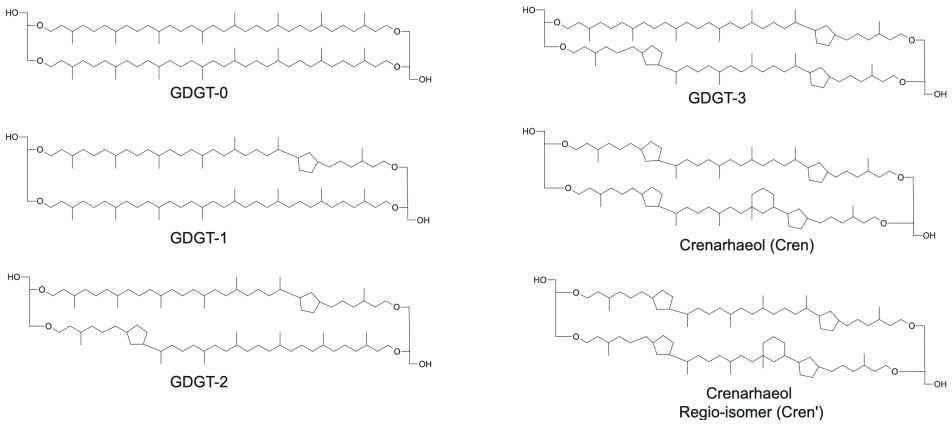

Figure. S1: Molecular structure of isoprenoid GDGTs.

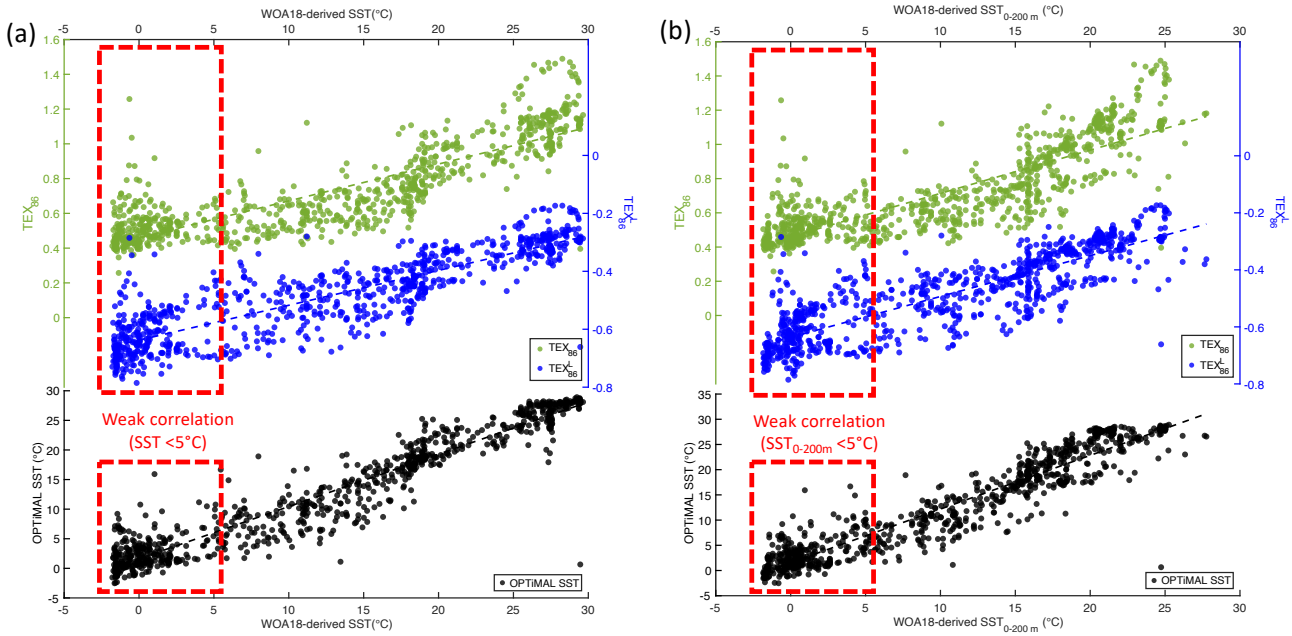

Figure. S2: Correlation of TEX_{86} index, TEX_{86}^{L} index, and OPTiMAL SST in the global core-top samples (n =859) with (a) WOA18-derived SST and (b) WOA18-derived $SST_{0\text{-}200m}$. Green circles: TEX_{86} index, blue circles: TEX_{86}^{L} index, black circles: OPTiMAL SST. Core-top samples are from Tierney and Tingley (2014), Jaeschke et al. (2017) and Lamping et al. (2021).

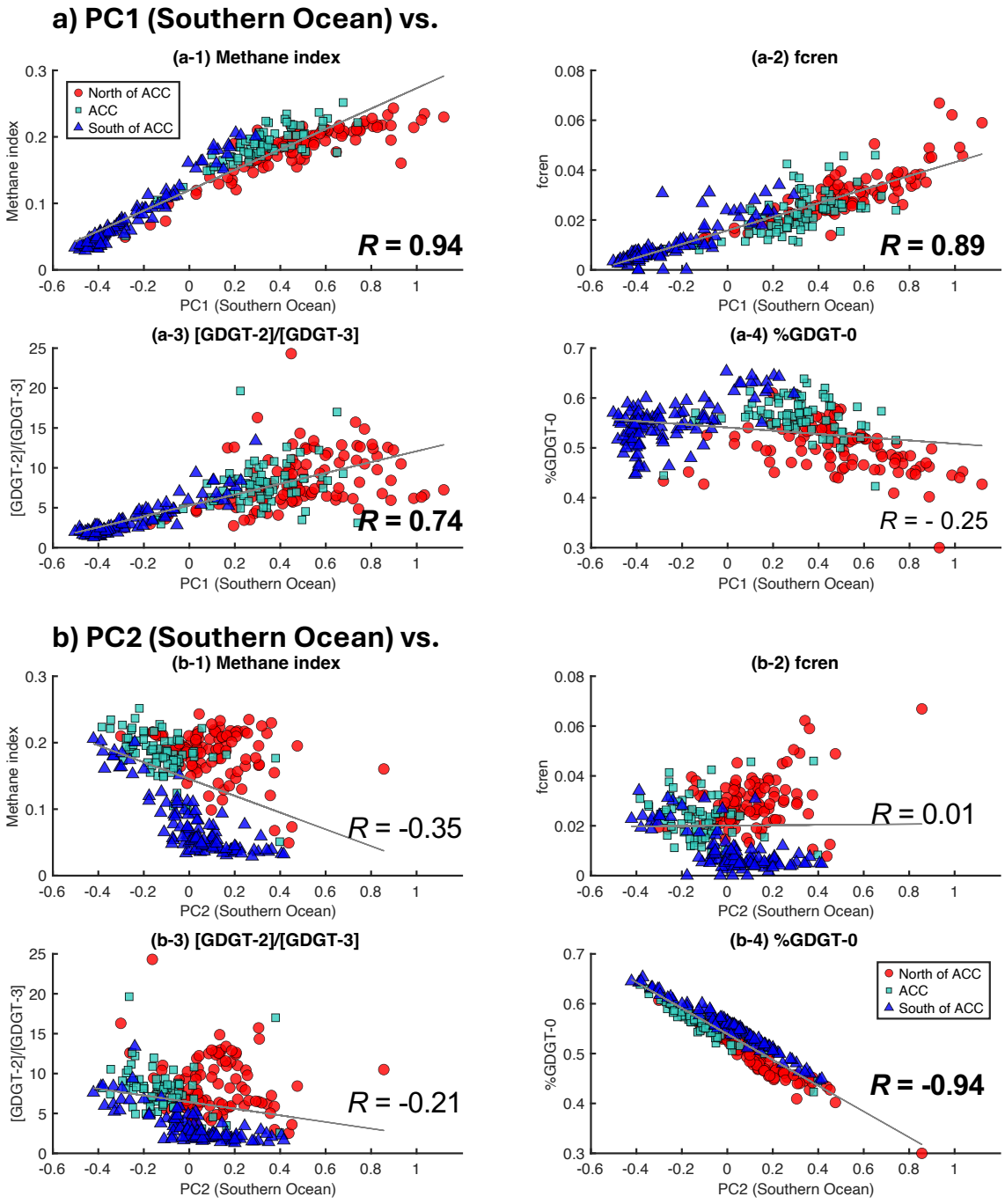

Figure S3: Scatter plots of (a) PC1 and (b) PC2 versus (1) Methane Index, (2) fcren, (3) [GDGT-2]/[GDGT-3], and (4) %GDGT-0 in Southern Ocean core-top isoGDGT data (n = 289). Core-top values are classified into three groups based on frontal positions: north or the ACC (red circles), centre of the ACC (teal square), and south of the ACC (blue triangle) as defined by the SBF and SAF (Fig. 4c). Core-top samples are from Tierney and Tingley (2014), Jaeschke et al. (2017) and Lamping et al. (2021).

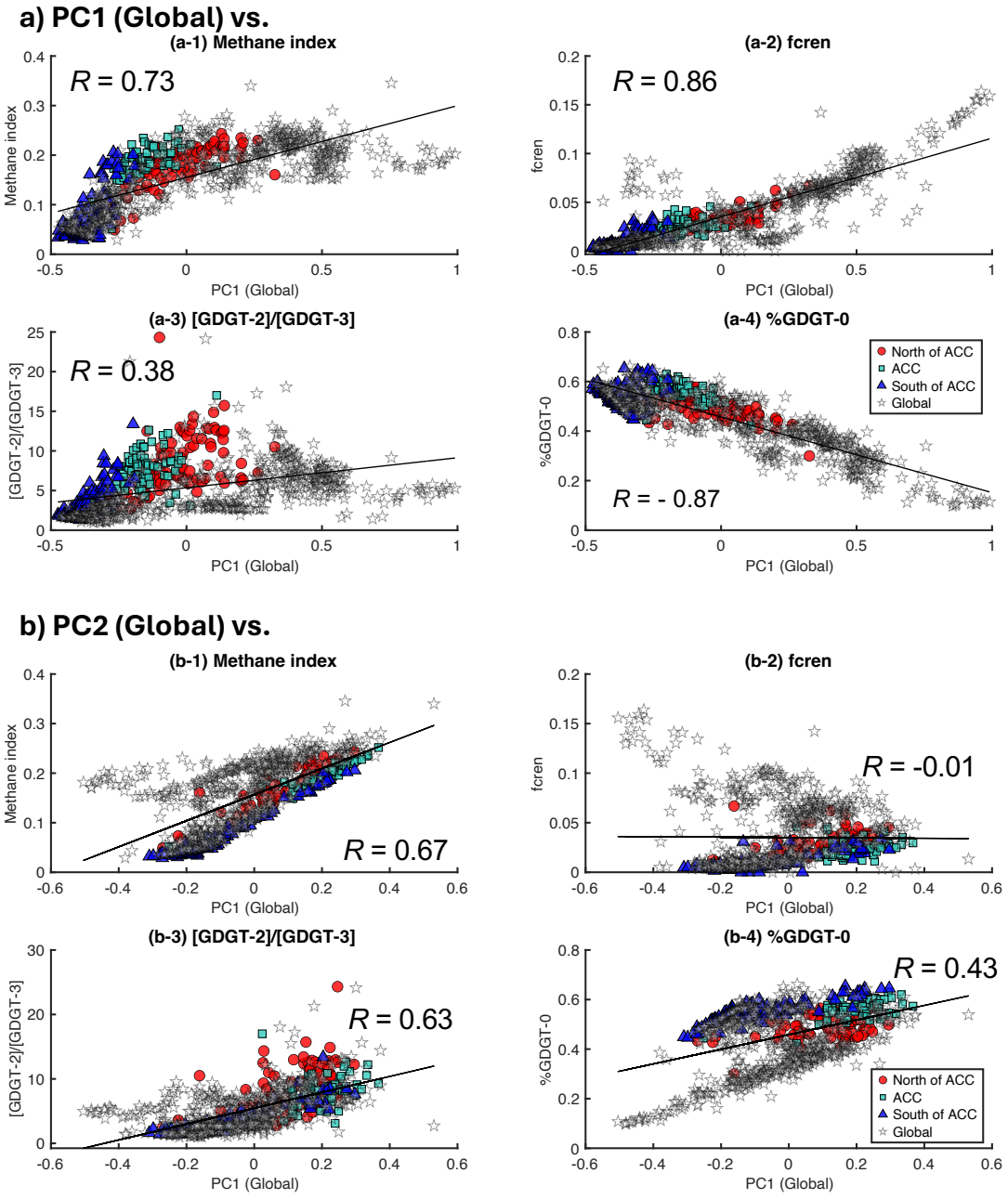

Figure. S4: Scatter plot of the global a) PC1 and b) PC2 versus (1) Methane Index, (2) fcren, (3) [GDGT-2]/[GDGT-3], (4) %GDGT-0 in the Global core top GDGT data (n = 916). The core-top values are classified into three groups: north or the ACC (red circles), centre of the ACC (teal square), and south of the ACC (blue triangle), as defined by the SBF and SAF (Fig. 4c). Core-top samples are from Tierney and Tingley (2014), Jaeschke et al. (2017) and Lamping et al. (2021).

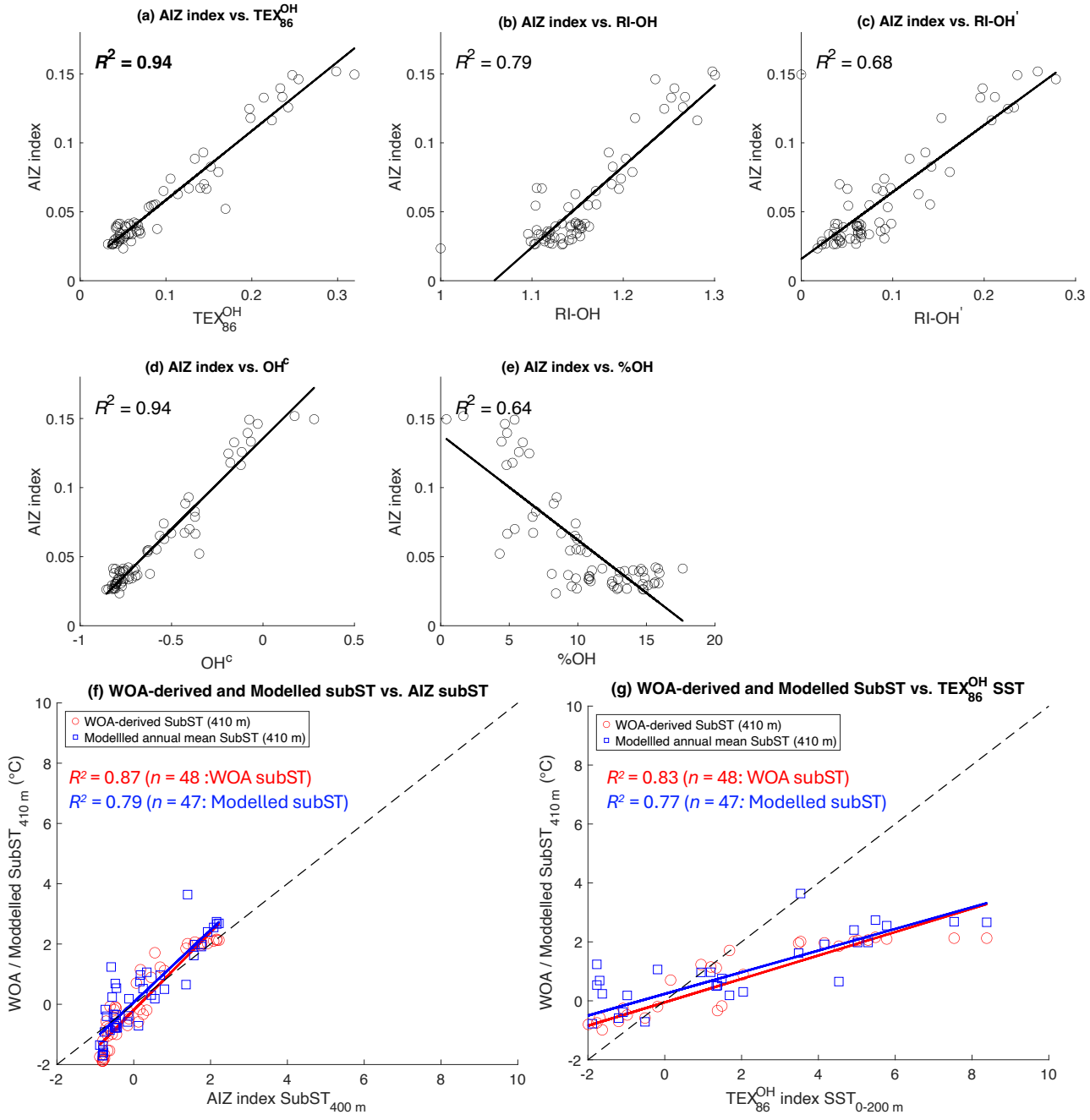

Figure. S5: Comparison of the AIZ index with OH-isoGDGTs-based indices. (a–e) Linear regression analyses between the AIZ index and OH-isoGDGT-based indices (TEX_{86}^{OH}, RI-OH, RI-OH', OHc, and %OHc) for sites where both isoGDGTs and OH-isoGDGTs are available (n = 66; data from Lamping et al., 2021). (f) AIZ-derived $subST_{400\ m}$ plotted against WOA-derived (red circles) and modelled (blue squares) subsurface temperatures at 41 0 m depth (temperature data from Lamping et al., 2021). (g) Same as (f) but for TEX_{86}^{OH}-derived $SST_{0–200\ m}$ instead of AIZ-derived $subST_{400\ m}$. Solid lines represent linear regressions and R^2 values shown. Gray dashed lines represent the 1:1 line.

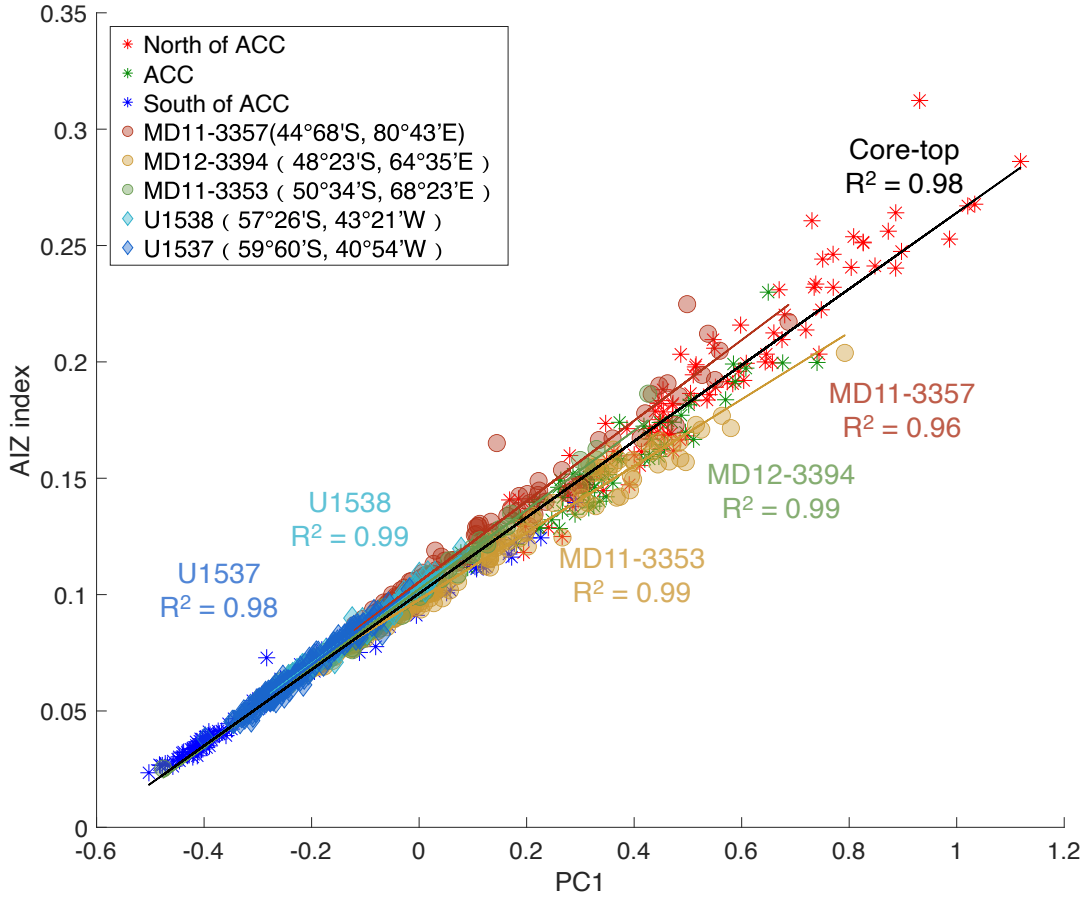

Figure. S6: Scatter plot of PC1 versus AIZ index in the Southern Ocean core-top samples and five sediment cores spanning the last 160 kyr. Core-top samples are classified by position relative to the ACC: red asterisks (north of the ACC), green asterisks (centre of the ACC), blue asterisks (south of the ACC). Sediment cores: dark red circles (MD11-3357), dark yellow circles (MD12-3394), green circles (MD11-3353), and light blue diamonds (U1538), blue diamonds (U1537). Core-top samples are from Tierney and Tingley (2014), Jaeschke et al. (2017) and Lamping et al. (2021). Sediment core data: MD11-3357 (Ai et al., 2024), MD12-3394 and MD11-3353 (Ai et al., 2020), U1538 and U1537 (this study).

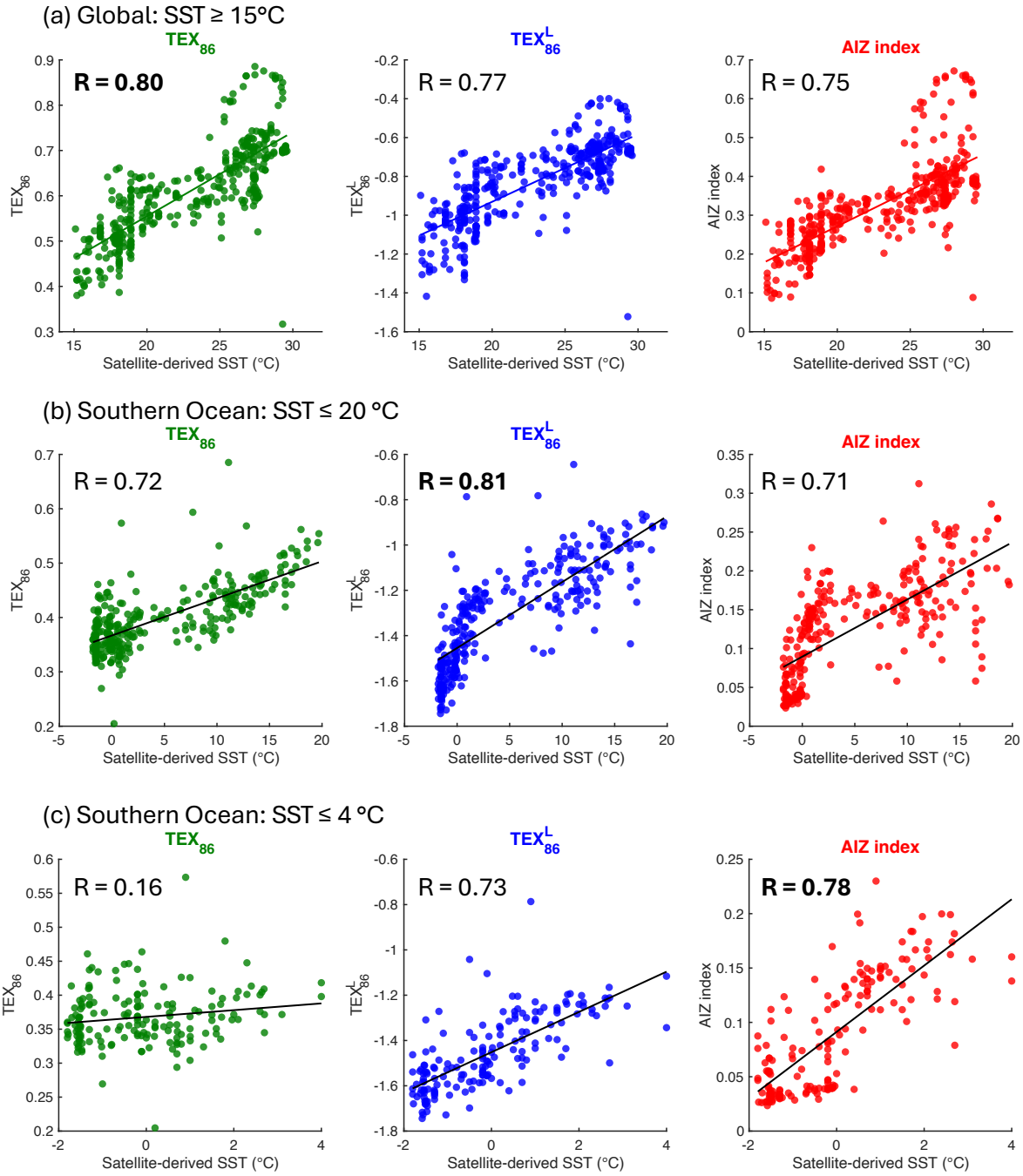

Figure. S7: Comparison of isoGDGT-based temperature proxies (TEX_{86}, TEX_{86}^{L}, and AIZ index) with satellite-derived SST across global and the Southern Ocean core-top datasets. Temperature ranges: (a) global sites ≥ 15 °C, (b) Southern Ocean sites ≤ 20 °C, and (c) Southern Ocean sites ≤ 4 °C. Symbols represent: green circles = TEX_{86}, blue circles = TEX_{86}^{L}, red circles = AIZ index (this study). Core-top samples are from Tierney and Tingley (2014), Jaeschke et al. (2017) and Lamping et al. (2021). SST are derived from the WOA18 0.25° × 0.25° gridded product (Boyer et al., 2018).

Table S1: Definitions of isoGDGT and hydroxylated isoGDGT-based proxy indices.

Proxy indices	**Reference**
$\mathrm{TEX}_{86}^{\mathrm{OH}} = \frac{[\mathrm{GDGT}-2]+[\mathrm{GDGT}-3]+[\mathrm{Cren}']}{[\mathrm{GDGT}-2]+[\mathrm{GDGT}-3]+[\mathrm{Cren}']+[\mathrm{OH}-0]}$ $\mathrm{TEX}_{86}^{\mathrm{OH}} = 0.025 \times \mathrm{SST}_{0-200\,\mathrm{m}} + 0.11$	Varma et al. (2025)
$\mathrm{RI}-\mathrm{OH} = \frac{[\mathrm{OH}-1]+2\times[\mathrm{OH}-2]}{[\mathrm{OH}-1]+[\mathrm{OH}-2]}$	Lü et al. (2015)
$\mathrm{RI}-\mathrm{OH}' = \frac{[\mathrm{OH}-1]+2\times[\mathrm{OH}-2]}{[\mathrm{OH}-0]+[\mathrm{OH}-1]+[\mathrm{OH}-2]}$	Lü et al. (2015)
$\mathrm{OH}^{\mathrm{C}} = \frac{[\mathrm{GDGT}-2]+[\mathrm{GDGT}-3]+[\mathrm{Cren}']+[\mathrm{OH}-0]}{[\mathrm{GDGT}-1]+[\mathrm{GDGT}-2]+[\mathrm{GDGT}-3]+[\mathrm{Cren}']+\sum[\mathrm{OH}-\mathrm{GDGTs}]}$	Fietz et al. (2016)
$\%\mathrm{OH} = \frac{\sum[\mathrm{OH}-\mathrm{GDGTs}]}{\sum[\mathrm{OH}-\mathrm{GDGTs}]+\sum[\mathrm{iso}-\mathrm{GDGTs}]}$	Huguet et al. (2013)